Research Article | Vol. 32, No. 10 / 6 May 2024 / Optics Express 17260
Optics EXPRESS

Analysis of short-term polarization stability using Allan variance

BORJA VIDAL*

Nanophotonics Technology Center, Universitat Politecnica de Valencia, Camino de Vera, sn, 46022, Valencia, Spain
*bvidal@dcom.upv.es

Abstract: The application of Allan variance to characterize the stability of optical signals affected by stochastic polarization fluctuations and the identification of the underlying power law noise processes is explored. Allan variance can ease the comparison regarding polarization stability of optical systems affected by polarization noise and define a near-optimum integration interval to reveal trends. Examples of the application of Allan variance to optical systems with stable polarization conditions show that white noise and random walk terms can be observed. Additionally, experiments show that the three Stokes parameters can exhibit different statistical behaviors in the Brownian-noise regime. Allan analysis can easily be used to define, in real-time systematically, the denoising strategy in polarization-based sensing and for the optimization of polarization-sensitive optical systems instead of the conventional approach relying on heuristics or information criteria.

1. Introduction

Electromagnetic waves are defined by three physical degrees of freedom: intensity, frequency and polarization. The performance of light-based systems relies on the precise determination of these properties. Optical amplitude noise processes have been thoroughly studied [1,2]. This knowledge allows the proper design of optical networks and photonic systems. Similarly, the frequency stability of laser oscillators has been extensively researched [3–5], enabling ultra-precise measurements in several fields of physics and opening new engineering applications such as satellite navigation and network synchronization.

The evolution of the state of polarization (SOP) of an optical signal, defined in the Jones or Stokes spaces, has been well studied [6]. In fiber optics, the polarization state of light fluctuates with time due to variations in wavelength or changes in birefringence, which is very sensitive to any nonsymmetric perturbation about the fiber axis that can be caused by varying environmental conditions such as temperature or mechanical changes. Considerable attention [6–10] has been devoted to describing polarization changes with frequency and, similarly, fiber length. However, modeling the impact of environmental perturbations on the time evolution of the SOP is challenging due to the lack of homogeneity of the problem [11–15].

To quantify the polarization stability of a signal, standard metrics are the rate of change of the SOP, i.e., the angular velocity in the Stokes space [13–15] for a fixed input SOP, which is suitable to quantify the magnitude of polarization transients amid polarization drifts; and the mean squared error of Stokes parameters [12], to assess changes from a given SOP.

Here, a tool initially developed to address frequency stability and synchronization issues between atomic clocks is applied to study the character of noise terms affecting polarization fluctuations in optical systems. Allan deviation, or variance, is a time-domain analysis technique designed to characterize noise by measuring the heterogeneity of its change across time. It is based on representing the root mean square (RMS) of an error signal as a function of averaging times, which has been extensively used to characterize the frequency stability of oscillators

#505502 https://doi.org/10.1364/OE.505502
Journal © 2024 Received 11 Sep 2023; revised 27 Jan 2024; accepted 21 Feb 2024; published 26 Apr 2024

Optics EXPRESS

[3,4]. This technique allows the characterization of the underlying random processes that drive stochastic fluctuations.

2. Polarization stability

The SOP of a light signal can be defined in the Stokes space as a vector, $\hat{s}$, which represents a point on the Poincaré sphere [6]. Changes in the SOP at the output of a system can be due to random changes in birefringence caused by the transduction of temperature fluctuations to the refractive index via the thermo-optic coefficient, stress and strain-induced changes in refractive index along different axes and also to changes in the wavelength of the optical signal or phase noise.

Fluctuations affecting the measured SOP, $\hat{s}_{meas}$, can be represented as errors on the polarization vector. Their aggregated magnitude, as a measure of the strength of the fluctuations, can be collapsed into a single factor by measuring how far each sample has deviated from its ideal position on the Poincaré sphere, $\hat{s}_{reference}$. This error, $\hat{s}_{error}$, [12], quantifies the level of fluctuations experienced by the signal. Thus, the amount of stochastic fluctuations on the instantaneous Stokes parameters can be estimated by calculating an error vector as the difference between the measured and ideal SOPs, as shown in Fig. 1.

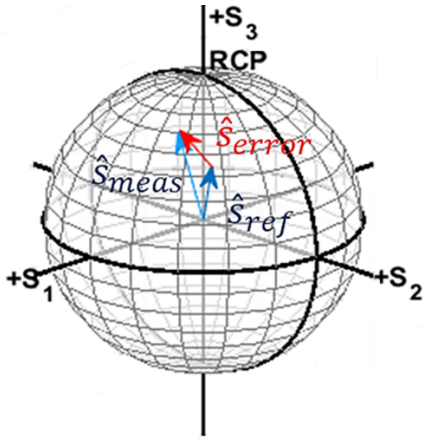

Fig. 1. Concept of polarization error vector (red) on the Poincaré sphere.

A factor can be defined to measure the accumulated error as the root mean square (rms) value of all the error vectors, averaged over N measurements [12],

$$|\hat{s}_{error}^{rms}| = \sqrt{\left(\frac{1}{3N}\right)\sum_{i=1}^{N}(S_{1,\,i} - S_{1,\,ref})^2 + (S_{2,\,i} - S_{2,\,ref})^2 + (S_{3,\,i} - S_{3,\,ref})^2} \tag{1}$$

where $S_{1..3}$ are the normalized Stokes parameters. This parameter eases the comparison among systems in terms of polarization stability as, for example, the conceptually similar error vector magnitude (EVM) parameter provides a system-level metric used to quantify the performance of digital modulations under varied impairments.

3. Analysis of polarization stability using Allan deviation

Some stochastic processes with scale-free dynamics have power spectral densities that follow a power law, i.e., their spectral density can be approximated by a sum of terms, each varying as an

Optics EXPRESS

integer power of frequency. A power law process has a spectral density of the form,

$$S(f) = \sum_{\alpha=-2}^{2} h_\alpha f^\alpha \tag{2}$$

where some terms of the summation are usually dominant. The PSD of each power-law process can be specified by its slope on a log-log plot for a given range of frequencies and its amplitude.

Through the estimation of the polarization stability provided by $|\hat{s}^{rms}_{error}|$, Allan deviation can be used to investigate the power-law noises affecting polarization fluctuations. Let be a set of N consecutive data points showing the instantaneous SOP error, $|\hat{s}^{rms}_{error}(t)|$, each sampled at time T_s, we can group n samples (with $n<N/2$) in a cluster. The temporal duration of each cluster, or the correlation time, is $\tau = n \cdot T_s$. The average for a cluster which starts from the k data point and contains n subsequent points is

$$\bar{y}_k = \frac{1}{\tau} \sum_{i=k}^{k+n} |\hat{s}^{rms}_{error}(i)| \tag{3}$$

Thus, Allan variance, $\sigma^2(\tau)$, is defined as half the averaged squared mean of two adjacent clusters,

$$\sigma^2(\tau) = \frac{1}{2} \langle (\bar{y}_{m+1} - \bar{y}_m)^2 \rangle \tag{4}$$

where $\langle \cdot \rangle$ denotes the average operator over all the clusters. It is a positive value and it can only be calculated for $\tau < \frac{N \cdot T_s}{2}$ or equally $n < \frac{N}{2}$. For large values of τ, the number of clusters is low, and consequently, the statistical error increases. To reduce the sizeable statistical error of standard Allan variance, more clusters can be obtained by overlapping samples among clusters [16]. First, the difference between two clusters each of n samples is calculated. Then, each cluster is shifted one sample and the difference calculated again. This process is repeated to obtain a more extensive set of averages. This method is known as the overlapping Allan variance. It shows better statistical error at the cost that clusters are no longer statistically independent.

Allan variance is related to the power spectral density, PSD, of the random process [17]. This relation is:

$$\sigma^2(\tau) = 4 \int_0^\infty S(f) \cdot \frac{sin^4(\pi f \tau)}{(\pi f \tau)^2} df \tag{5}$$

where $S(f)$ is the PSD of $|\hat{s}^{rms}_{error}(t)|$. From (5) it can be seen that Allan variance is proportional to the total power output of the random process after being filtered by a frequency response given by $sin^4(\pi f \tau)/(\pi f \tau)^2$. In other words, Allan variance can be calculated in the time domain as a convolution (4) or in the frequency domain as a filter (5). The bandwidth of the filter depends on τ, thus, the different types of underlying noise terms in the signal can be identified and quantified by varying τ. This is usually done through a log-log plot of $\sigma(\tau)$ versus correlation time which allows to sort out noise components by the slopes of Allan deviation [18].

Experiments have been carried out to study polarization using Allan analysis. Two polarimeters have been used through the experiments: polarimeter #1 (Optellios PS2300B) and polarimeter #2 (Thorlabs PAX1000IR2/M). As an example of application, Figs. 2(b),(c) show logarithmic plots of Allan deviation for the change in polarization during short time windows obtained with a light source connected to polarimeter #1 through a polarization controller (Fig. 2(a)) during regular operation (Fig. 2(b)) and during laser warming-up (Fig. 2(c)). Figures 2(d),(e) show the temporal evolution of Stokes parameters and their Poincaré sphere representation. Measurements were carried out with a sampling rate of the polarimeter of 200 Hz. The number of samples was 10000 in all experiments. For convenience, the first data point is selected as the reference SOP.

Several piecewise linear regions with different slopes can be observed in the two examples shown in Fig. 2(b),(c). These straight lines on the log plot are potential signatures of a power law. From the figure, the main types of dominant error can be identified.

Optics EXPRESS

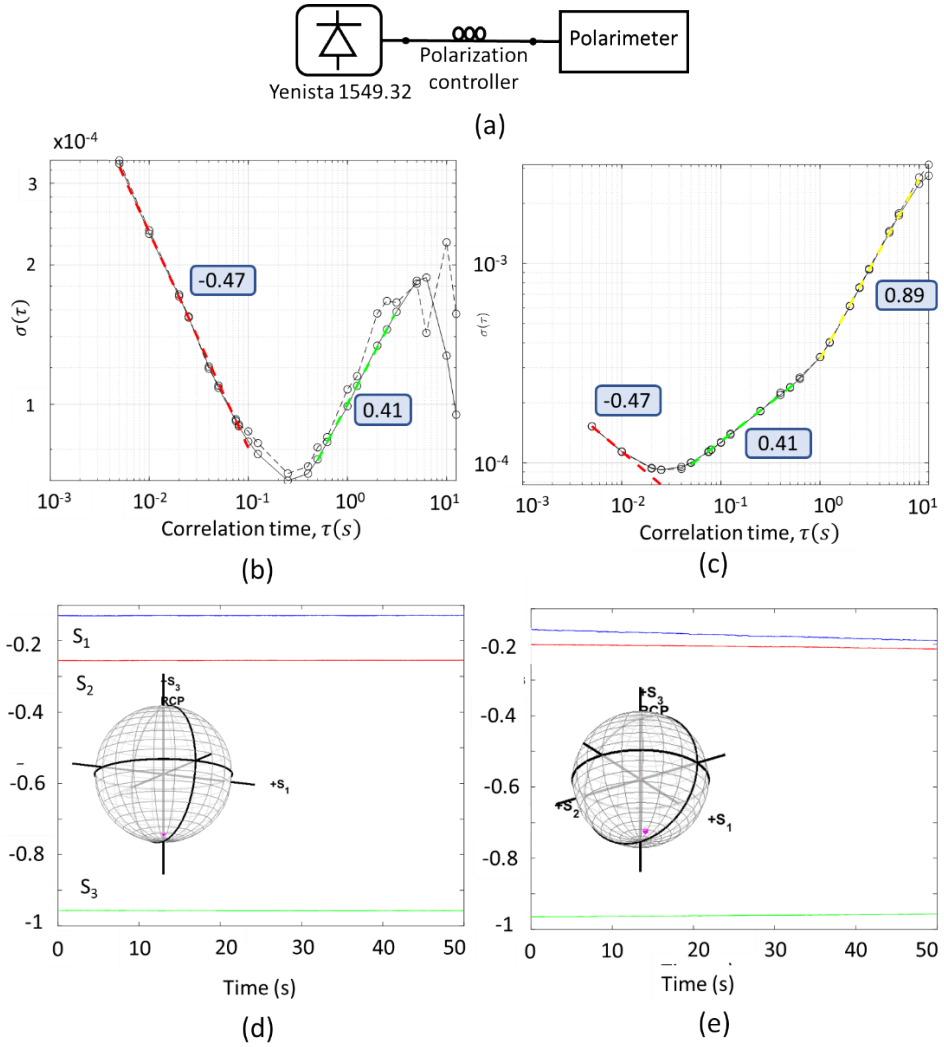

Fig. 2. Application of Allan deviation to SOP analysis. (a) Experimental setup Yenista laser (model 1549.32) connected to polarimeter #1 through a polarization controller. Log-log plot of Allan deviation for regular operation (b) and laser warming-up (c), where (dashed) corresponds to the non-overlapping estimator and (solid) to the overlapping one; red, green, and yellow dashed lines are linear regression fits. The time evolution of the sampled Stokes parameters is shown in (d), (e) where the insets provide the representation on the Poincaré sphere.

Optics EXPRESS

The downward slope, with a slope of $-1/2$, can be associated to white noise following Allan analysis theory. This noise can arise from several contributions. It can be caused by random fluctuations in the local birefringence due to vibrations [6], rapid laser frequency noise attributed to the inherent linewidth resulting from spontaneous emission, operating within time scales faster than the microsecond [19], the unpolarized component of the signal from the optical source, and the optoelectronic noise of the photodetection in the polarimeter. The accumulated effect of all these perturbations gives rise to high-frequency random changes on the recorded SOP with a correlation time much shorter than the sampling time, and they can be characterized by a white noise spectrum.

$$S(f) = N_0^2 \tag{6}$$

Substituting (6) in (5), the Allan deviation yields,

$$\sigma(\tau) = \frac{N_0}{\sqrt{\tau}} \tag{7}$$

Thus, the Allan deviation of the white noise term can be derived, showing a slope of $-1/2$. This is observed in the experimental data shown in Fig. 2(b),(d), whose slope was calculated through a linear regression. The strength of the noise term can be quantified by reading the value at $\tau = 1$ of the linear fit of the data.

Figure 3 shows the experimental data for the white noise term of Fig. 2(b), simulations of a discrete white noise process with the same standard deviation as the one derived from Allan analysis and a linear fit to the data, which has a R^2 value of 0.9987.

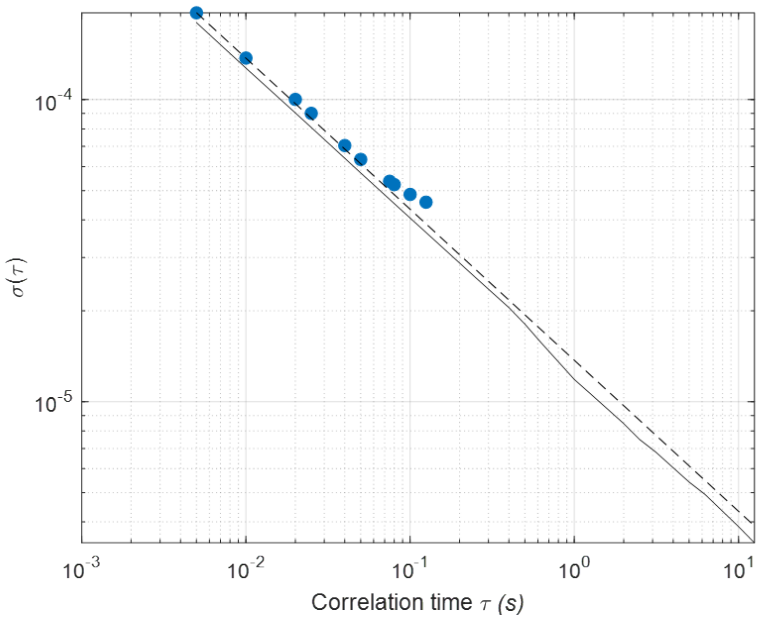

Fig. 3. Overlapping Allan deviation, $\sigma(\tau)$, for the white noise term on a log-log plot: Allan deviation calculated from white noise simulations with parameters from Fig. 2(b) (solid black); Theoretical linear fit with -0.5 slope (dashed black); Experimental results from Fig. 2(b) (blue dots).

The white noise term seems to have several main contributions. One is related to the noise floor of the polarimeter. Measurements under stable conditions and high signal to noise ratio point out that the polarimeters have a noise floor of the N_0 coefficient that can be estimated to

Optics EXPRESS

be $N_0^{\#1} = (1.7 \pm 0.3) \cdot 10^{-5}$ and $N_0^{\#2} = (0.61 \pm 0.06) \cdot 10^{-5}$, respectively. Fluctuations caused by environmental and wavelength changes increase the recorded white noise term. This white continuous polarization noise is filtered by the analog bandwidth of the polarimeter. Figure 4 shows the Allan deviation for an optical source connected through a SMF28 fiber and a fiber splitter to both polarimeters. The fiber section was 20-meter long unspooled and it was laid in the floor untapped. The magnitudes of the white noise term in this case are $N_0^{\#1} = 19.4 \cdot 10^{-5}$ and $N_0^{\#2} = 22.16 \cdot 10^{-5}$. The small difference in the magnitude of the white term can be caused by the fact that polarimeter #2 has wider bandwidth. The measured values of N_0 should be interpreted as upper bounds since quantization of the Stokes parameters by the polarimeter might introduce an additional white noise term (Supplement 1).

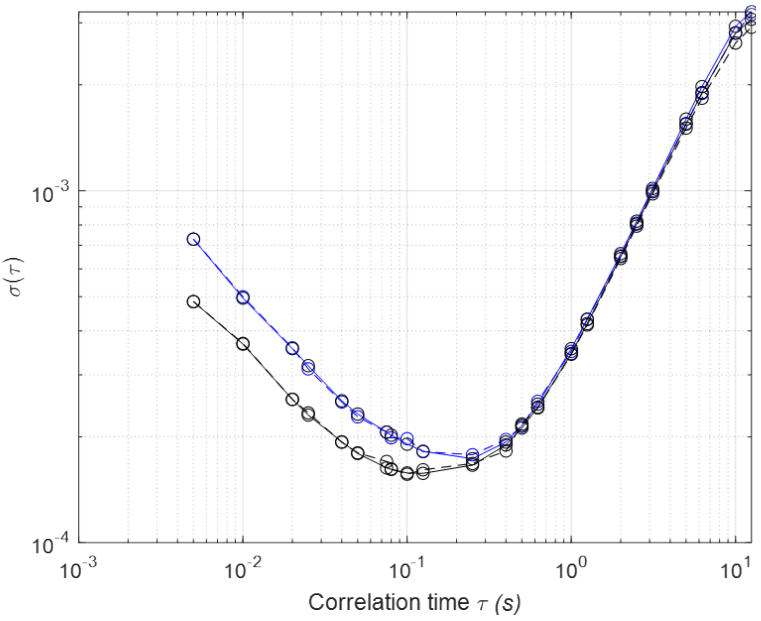

Fig. 4. Log-log plot of Allan deviation for the non-overlapping estimator (dashed) and to the overlapping one (solid) for two polarimeters: #1 Optellios PS2300B (black) and #2 Thorlabs PAX1000IR2/M (blue).

Finally, the contribution from the unpolarized component of the signal increases the white term coefficient. Figure 5 shows N_0 values for different optical power levels of an optical carrier related to the degree of polarization (DOP). It can be seen how the white noise term increases as the degree of polarization decays, showing a linear relation with a $R^2 = 0.986$.

An upward slope can be observed in Fig. 2(b),(c). It can be associated with a low-frequency drift, i.e., noise that changes over longer time frames and, therefore, starts to affect larger data clusters. These SOP fluctuations can be induced by slow changes in the SOP of the source and changes in the magnitude or orientation of the PMD vector by temperature changes or other slow-varying perturbations along the fiber [6]. Given the range of slopes observed, it can be interpreted as a fractional Brownian motion (fBm) noise [20], i.e., a Gaussian zero-mean nonstationary stochastic process with stationary increments and which is defined by the Hurst exponent, H, which goes from 0 to 1 and is directly related to the slope of Allan deviation on the log plot. This noise is an extension of ordinary Brownian noise, obtained for $H = 1/2$. Values $H<1/2$ result in a mean-reverting process (antipersistent), whereas $H>1/2$ reflect a process that has a trend (bias) with the value of $H = 1$ corresponding to a bias instability, or, in other words,

Optics EXPRESS

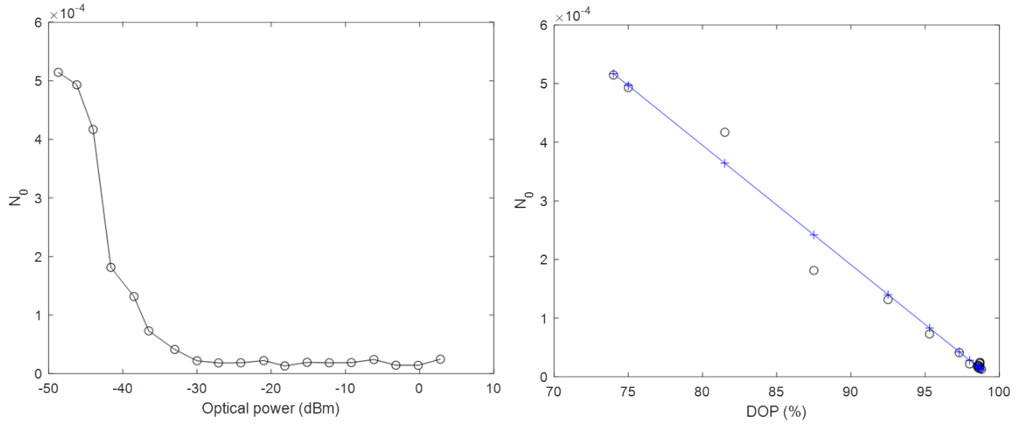

Fig. 5. (a) White noise coefficient, N_0, as a function of the optical power, and (b) relation between white noise coefficient and degree of polarization (DOP) in both cases for polarimeter #1.

the closest that H is to 1 the greater the degree of persistence or long-range dependence, i.e. the evolution of the SOP shows statistically significant correlations across large time scales. In the study of polarization evolution, it could be associated with the total birefringence of the system. Several models of polarization evolution in optical fibers with propagation length or frequency rely on having the PMD vector change orientation randomly as a random walk [6,7].

In particular, for the system described in Fig. 2(a), the slope is around $+1/2$ on the log—log plot following the dynamics of Brownian noise, i.e. the short time future evolution of SOP cannot be predicted since values are uncorrelated. This random polarization drift can be interpreted as a continuous Wiener process that is being discretized by the polarimeter, becoming a random walk. It is a nonstationary process that manifests as impulsive changes on the SOP. The random walk (Brownian) nature of the noise means that there is no memory or correlation from one impulse to the next. These discrete random disturbances can be described as a set of random steps on the mathematical space of the Poincaré sphere. The PSD of a random walk noise is [17]

$$S(f) = \frac{K^2}{(2\pi f)^2} \tag{8}$$

The standard deviation associated with a random walk noise can be obtained by substituting (8) into (5). It can be expressed as

$$\sigma(\tau) = K\sqrt{\frac{\tau}{3}} \tag{9}$$

where K is the random walk coefficient. The magnitude of this term can be read from the fit slope line at $\tau = 3$.

The magnitude of the noise term of Fig. 2(c) is $K^{(a)} = (1.7 \pm 0.7) \cdot 10^{-4}$. Figure 6 compares the measurement of Fig. 2(c), the theoretical slope $(+1/2)$ and simulations of Brownian noise. The goodness-of-fit measure through R^2 shows a value of 0.9942, pointing out, as in the white noise term, the plausibility of a power law as a fit of the data. In both cases Allan analysis allows the identification of the dominant noise term within the measurement window. Figure 6 shows a decrease for large averaging (correlation) time, partially replicated in simulations. It seems related to the sample size (10000 samples in both simulations and experiments) since simulations show that when using a more significant number of samples, the curve tends to be the theoretical linear slope.

Optics EXPRESS

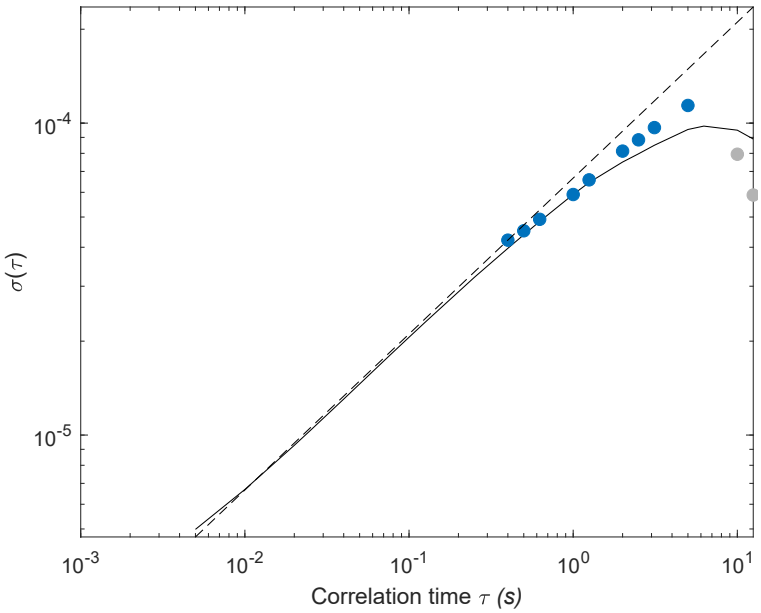

Fig. 6. Overlapping Allan deviation, $\sigma(\tau)$, for the random walk term on a log-log plot: Allan deviation calculated from simulations of Brownian noise on a sphere with the same coefficient as measurements from Fig. 2(b) (solid black); Theoretical linear fit with 0.5 slope (dashed black); Experimental results shown in Fig. 2(b) (blue dots).

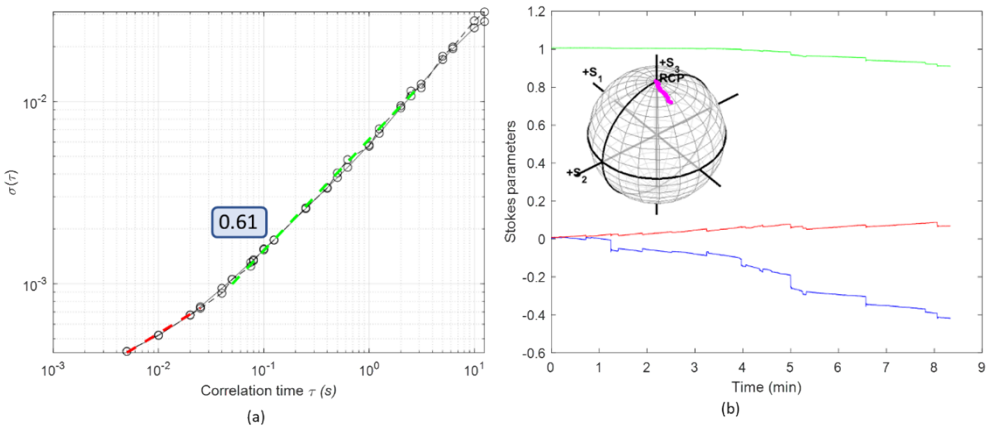

Fig. 7. (a) Log-log plot of Allan deviation. (Dashed) non-overlapping estimator, (solid) overlapping estimator; red and green dashed lines are linear regression fits; (b) Evolution of the sampled Stokes parameters, blue, red, and green represents S1, S2, and S_3 respectively, (inset) Poincaré sphere representation.

Optics EXPRESS

Figure 7(a) shows Allan deviation for an experiment where a different optical source (HP8168F) was connected through a 20m-long uncoiled standard single-mode fiber to polarimeter #1. In this case, the slope (Hurst exponent) is 0.61, i.e., close to the dynamics of Brownian noise. Still, the magnitude of the Brownian term, K, is 70 times the one of Fig. 2(a). The poorer stability of this dataset can be qualitatively appreciated through the time evolution of Stokes parameters as seen in Fig. 7(b). Thus, Allan analysis can be used not only to identify but also to quantify polarization fluctuations.

Finally, Fig. 2(c) shows a second upward slope. It has a slope close to 1, and thus, it points out the presence of a trend, i.e., the system in the time scale of the measurement is evolving through a systematic (deterministic) bias. Figure 8 shows an Allan deviation plot for an optical source connected to polarimeter #1 with a sampling rate of 10 Hz through a polarization controller and a DGD module (90 ps). The polarization controller controls the SOP at the input of the DGD to be at 45° of its axes. In Fig. 8, a slope close to unity can also be observed. This can be attributed to the precession of the SOP around the PMD vector axis at a rate governed by the strength of the birefringence under slow frequency drifts (on longer observation times of the order of milliseconds or more), due to laser cavity fluctuations of various types and which are likely to be flicker $(1/f)$ [19]. This evolution can also be seen in the inset of Fig. 7(b) as an arc caused by the system strong birefringence (90 ps).

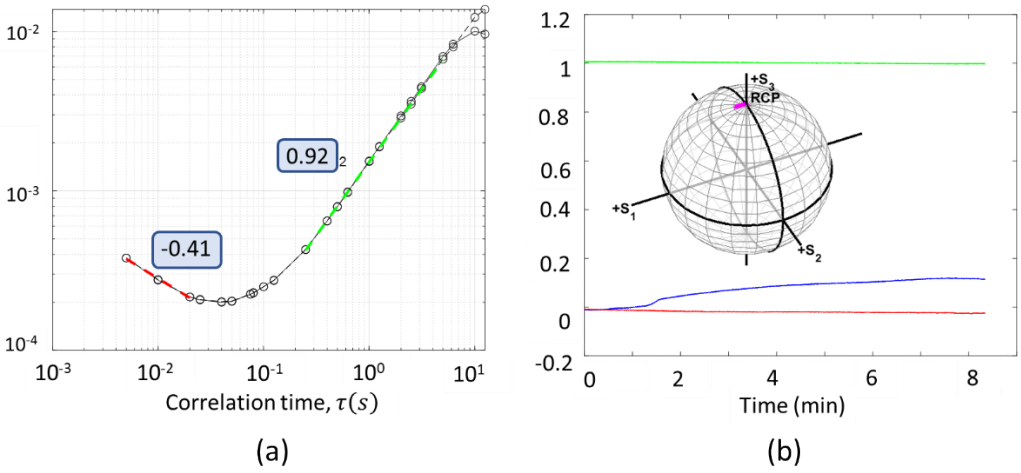

Fig. 8. (a) Log-log plot of Allan deviation. (Dashed) non-overlapping estimator, (solid) overlapping estimator; red and green dashed lines are linear regression fits; (b) Evolution of the sampled Stokes parameters, blue, red, and green represents S1, S2, and S_3 respectively, (inset) Poincaré sphere representation.

Allan deviation plots show a sweet spot where the standard deviation is minimized due to the averaging of fast-oscillating noise. In contrast, the data are not corrupted yet by slower polarization drifts. When a moving average analysis is carried out, the window length is critical in the performance of the estimator. Instead of evaluating multiple window lengths to select the near-optimal using heuristics or even information theory such as Akaike Information Criteria (AIC), Allan deviation provides a systematic data-driven method to determine the timescale over which the SOP remains relevant while minimizing white noise corruption of the nonstationary term. This is done without prior knowledge about the system or its noise model. For example, for the dataset shown in Fig. 2(b), a correlation time of $\tau = 0.25$ allows SOP variance to be minimized.

Optics EXPRESS

Figure 9 shows simulations of a small amplitude cosine signal embedded in additive white Gaussian noise. Allan analysis shows that the near-optimum length of the moving average filter is 200 samples. This value defines the window length of the optimum moving average filter that better retrieves information buried in noise for the dataset, i.e., a better estimation of the underlying deterministic component. As a comparison, the sum of the squared estimate of errors (SSE) for the measurement (50000 samples) goes from 2000 without averaging to 9 for a moving average of 200 samples. For an averaging window of 10 and 1000 samples, the SSE is 174 and 19, respectively.

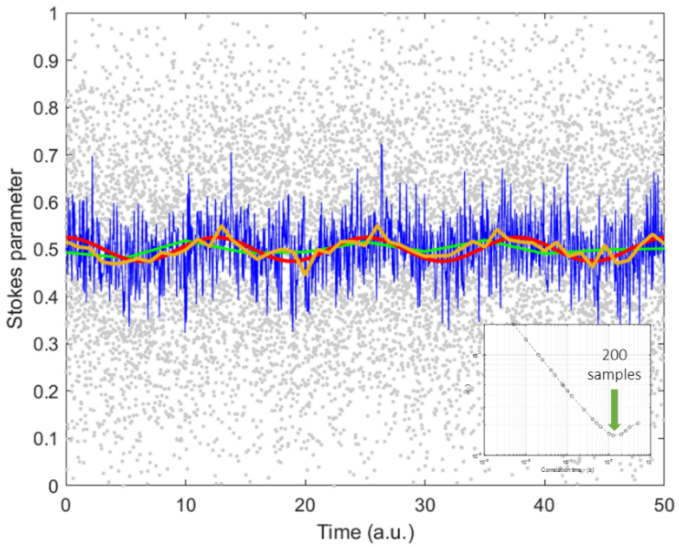

Fig. 9. Simulation of the evolution of a Stokes parameter driven by white Gaussian noise plus a small-amplitude cosine signal (red solid) sampled at 200 Hz. Evolution of the Stokes parameter (grey dots); moving average with window length 10 samples (blue solid); moving average with window length 200 samples, optimum point according to Allan deviation plot (orange solid); moving average with window length 1000 samples (green solid). Inset: Allan deviation plot of the Stokes parameter simulations.

Figure 10 shows simulations and measurements of a Stokes parameter under noise and polarimeter quantization and how the underlying noise term (random walk) is revealed when quantized white noise is removed through optimum moving average filtering with the window length given by Allan analysis. Since white noise is more significant than quantization noise, digitalization introduces an offset on the Allan curve and, consequently, the noise coefficients associated with each noise term. Still, it does not significantly change the optimum moving average filter length.

Finally, the application of Allan deviation to each Stokes parameter allows the comparison among their statistical behaviors or, from a geometrical point of view, the study of the isotropic nature of the noise terms on the Poincaré sphere. For example, Fig. 11 shows the Allan deviation for each Stokes parameter for two systems. A similar trend is obtained in spherical coordinates. On short time windows, the slope of the fractional Brownian noise term is different for each Stokes parameter. So, fluctuations are anisotropic, i.e., not all possible orientations of the error term of the Stokes vector are equally likely. The white noise term is very similar in slope and magnitude, although changes in magnitude can also be found. Figure 12 shows the time evolution of the coefficient of variation of the slope of the fractional Brownian noise component for different fiber lengths. The coefficient of variation has been chosen as a statistical measure to compare

Optics EXPRESS

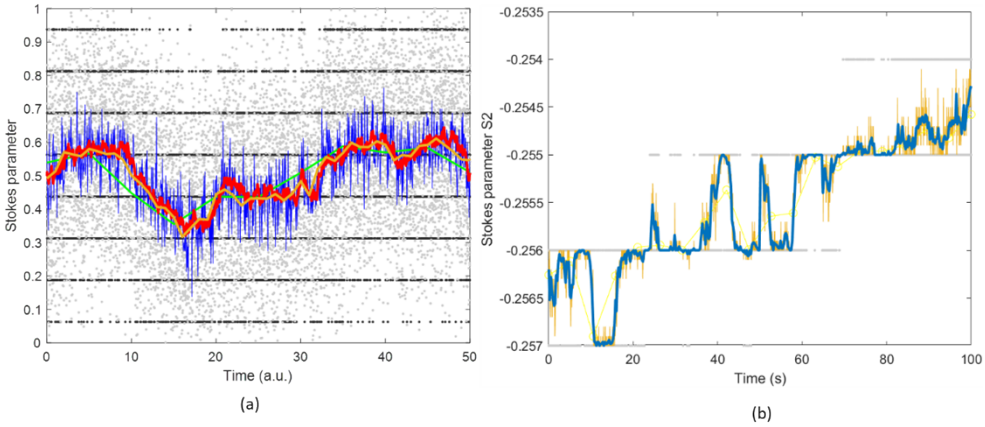

Fig. 10. (a) Simulation of the evolution of a Stokes parameter under Brownian noise (red), recorded value under white noise (light grey) plus quantization (dark grey dots), estimations of the evolution with different moving average windows lengths (blue: 10 samples; green: 1000 samples; orange: optimum value, 200, given by Allan analysis); (b) Experimental evolution of the quantized S_2 Stokes parameter (grey dots); estimation of the unknown evolution through the moving average with optimum window length (50 samples or 0.25 s) (blue solid); estimation through a moving average with window length 10 samples (orange solid).

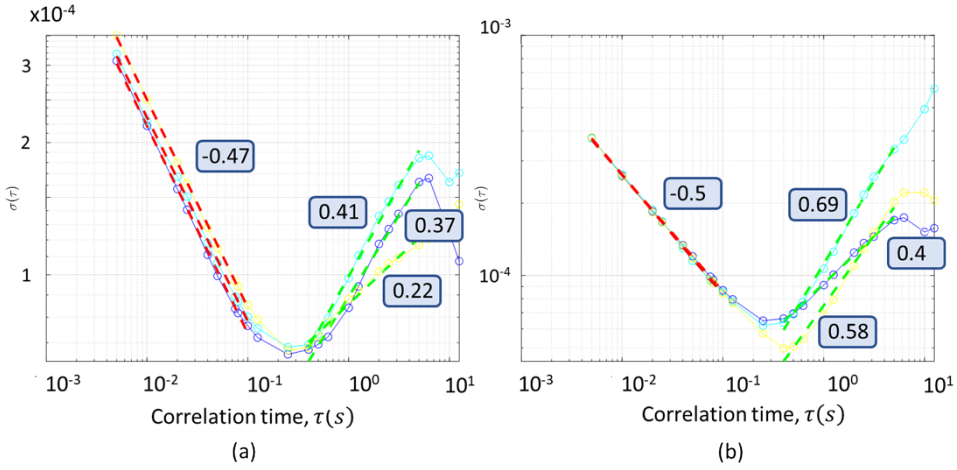

Fig. 11. Overlapping Allan deviation for each Stokes parameter in a 1 m standard single mode fiber measured with polarimeter #1 with 200 Hz sampling: S_1 (blue), S_2 (cyan), S_3 (yellow). (a) Measurement of Fig. 2(b); (b) Laser Keysight 81940A.

Optics EXPRESS

the other cases. Figure 12 shows spikes in which the slopes of each Stokes parameter differ and that with longer fiber lengths, these fluctuations are less frequent and less pronounced. This is aligned with previous works showing that SOP angular increments can be seen as a random walk equally likely in all directions [13] since as the fiber length increases, the diffusion of SOP angular increments would approach a uniform angular distribution related to the averaging of rotations of the local birefringence and thus the noise should converge to the same slope and magnitude.

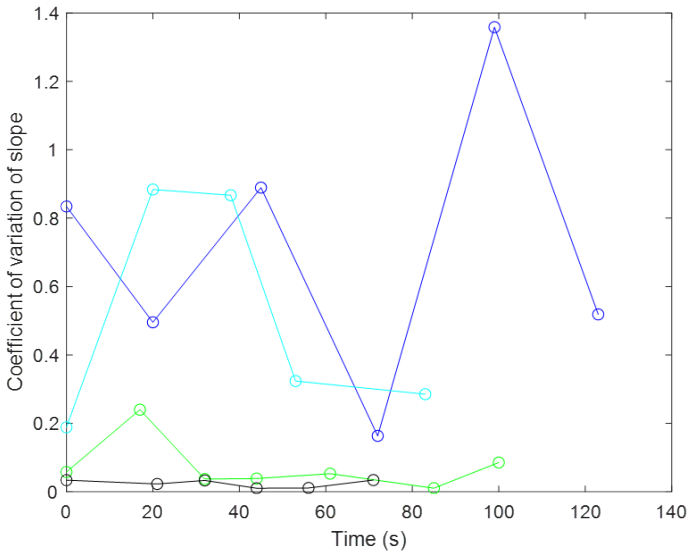

Fig. 12. Time evolution of the coefficient of variation of the slopes of each Stokes parameter measured with polarimeter #2 at 200 Hz for different fiber lengths: 1 m (blue); 20 m (cyan); 350 m (green); 1 km (black).

Table 1 shows the coefficient of variation of the slopes of each Stokes parameter for different cases measured with polarimeter #1. In particular, they correspond to two optical sources combined with other sections of standard single-mode fiber: 1-meter, 20-meter, and 350-meter-long sections of unspooled fiber and a 1 km-long fiber reel, respectively. There seems to be a trend towards reducing the slope variation among stokes parameters for longer fiber lengths.

Table 1. The median of the coefficient of variation for the slope for the fBm component among Stokes parameters for different lengths of standard single-mode fiber and sampling frequency

Length (m)	200 Hz sampling	10 Hz sampling
1	0.24	0.27
20	0.13	0.08
350	0.15	0.01
1000	0.05	0.23

4. Conclusion and discussion

The use of Allan deviation, a simple data-driven method available in most scientific software packages, for the analysis of stochastic polarization time fluctuations as a tool to study underlying noise models and the optimization of denoising in polarization measurements has been proposed

Optics EXPRESS

and studied. Allan analysis shows that short-time SOP evolution scale with multiple scaling rules rather than following a global scaling rule. Experiments have been conducted, and in them, the results are consistent with the hypothesis that the SOP evolves following a power law with different regimes, and thus different regularity patterns have been observed: a white noise term, i.e., a mean reverting (anti persistent) process; a random walk; and a fractional Brownian process that in the extreme develops in a trending (persistent) process. These short-time temporal noise terms agree with previously reported statistical models for the evolution of polarization with fiber length and optical frequency, which suggest that the changes in the PMD vector are driven by changes in orientation following a Brownian motion and a white rotation process [6,7]. Somewhat unexpectedly, experimental results show that each Stokes parameter might have a different statistical dynamic in the Brownian regime. However, this anisotropy seems to decrease as the fiber length is increased.

Allan deviation provides a systematic approach to selecting the time window length for averaging over which measurements remain relevant. If polarization fluctuations follow a power law, they are scale-invariant, or, in other words, they are self-similar. This implies no restrictions on the sampling frequency selection since the characteristics of the processes are conserved at different time scales.

Allan analysis is similar to other statistical tools but provides unique features. While both Allan analysis and power spectral density (PSD) provide insights into the frequency content and noise properties of a signal, Allan variance offers additional information related to noise characterization, stability analysis, and optimal averaging times that cannot be directly obtained from PSD alone. An alternative path for analyzing the regularity of polarization fluctuations could be in the framework of multifractal analysis (or scaling analysis). SOP fluctuations can be seen as a multifractal behavior with several dominant monofractal colored noise terms. Fractal structures similarly allow the identification of power law processes. However, multifractal tools such as leader wavelets and multifractal detrended fluctuation analysis do not provide a simple derivation of the optimum time window for denoising, and they are not as easy to use.

Allan analysis can contribute to advancing the study of systems where the time evolution of the SOP is relevant, such as in the optimization of the averaging in polarization measurements, comparison of optical systems in terms of polarization stability, modeling, and quantifying noise stemming from various sources as well as to provide new insights on the polarization behavior of optical systems. Different applications may benefit from Allan analysis, such as the optimization of polarimetric sensing, especially at low signal power [21], as in remote sensing [22] and astronomy [23]; the calibration of polarization elements, characterization of materials [24] and characterization of polarization speckle [25]; as well as the alignment of polarization-critical optical systems, as in quantum key distribution systems [26], microwave photonics [27] and fiber-optic gyroscopes [28]. This tool might strengthen the accuracy of these applications with an analysis that can be done on the fly to determine optimal parameters.

Funding. Ministerio de Ciencia, Innovación y Universidades (PID2019-111339GBI00).

Disclosures. The author declares no competing interests.

Data availability. Data underlying the results presented in this paper are not publicly available at this time but may be obtained from the author upon reasonable request.

Supplemental document. See Supplement 1 for supporting content.

References

1. G.P. Agrawal, *Fiber-optic Communication Systems*, Ed. (Wiley, 2010).
2. F. Czerwinski, A.C. Richardson, and L.B. Oddershede, "Quantifying Noise in Optical Tweezers by Allan Variance," Opt. Express **17**(15), 13255 (2009).
3. F.L. Walls and D.W. Allan, "Measurements of frequency stability," Proc. IEEE **74**(1), 162–168 (1986).
4. W. Riley and D.A. Howe, *Handbook of Frequency Stability Analysis*, (NIST, 2008).
5. Th. Udem, R. Holzwarth, and T. W. Hänsch, "Optical frequency metrology," Nature **416**(6877), 233–237 (2002).

Optics EXPRESS

6. X.S. Yao and X.J. Chen, *Polarization Measurement and Control in Optical Fiber Communications and Sensor Systems*, Ed. (John Wiley & Sons, 2023), Chap 3.
7. G.J. Foschini and C.D. Poole, "Statistical Theory of Polarization Dispersion in Single Mode Fibers," J. Lightwave Technol. **9**(11), 1439–1456 (1991).
8. J.P. Gordon and H. Kogelnik, "PMD fundamentals: Polarization mode dispersion in optical fibers," Proc. Natl. Acad. Sci. **97**(9), 4541–4550 (2000).
9. M. Karlsson, J. Brendel, and P.A. Andrekson, "Long-term Measurement of PMD and Polarization Drift in Installed Fibers," J. Lightwave Technol. **18**(7), 941–951 (2000).
10. A. Galtarossa, L. Palmieri, M. Schiano, *et al.*, "Statistical characterization of fiber random birefringence," Opt. Lett. **25**(18), 1322–1324 (2000).
11. P.J. Leo, G.R. Gray, G.J. Simer, *et al.*, "State of polarization changes: classification and measurement," J. Lightwave Technol. **21**(10), 2189–2193 (2003).
12. G. Soliman, M. Reimer, and D. Yevick, "Measurement and simulation of polarization transients in dispersion compensation modules," J. Opt. Soc. Am. A **27**(12), 2532–2541 (2010).
13. C.B. Czegledi, M. Karlsson, E. Agreli, *et al.*, "Polarization Drift Channel Model for Coherent Fiber-Optic System," Sci. Rep. **6**(1), 21217 (2016).
14. D. Charlton, S. Clarke, D. Doucet, *et al.*, "Field measurements of SOP transients in OPGW, with time and location correlation to lightning strikes," Opt. Express **25**(9), 285636 (2017).
15. D.L. Peterson, B.C. Ward, K.B. Rochford, *et al.*, "Polarization mode dispersion compensator field trial and field fiber characterization," Opt. Express **10**(14), 614 (2002).
16. D.A. Howe, D.U. Allan, and J.A. Barnes, "Properties of signal sources and measurement methods," *Thirty-Fifth Annual Frequency Control Symposium, Philadelphia (USA)*, (1981).
17. H. Hou, "Modeling inertial sensors errors using Allan variance," Master Thesis, University of Calgary, 2004.
18. N.J. Kasdin, "Discrete simulation of colored noise and stochastic processes and $1/f^{\alpha}$ power law noise generation," Proc. IEEE **83**(5), 802–827 (1995).
19. X. Ma and X.S. Yao, "Single frequency lasers' linewidth elegantly characterized with Sigmoid functions of observation time," arXiv, arXiv:2309.08885, (2023).
20. B.B. Mandelbrot and J.W. van Ness, "Fractional Brownian motions, fractional noises, and applications," SIAM Rev. **10**(4), 422–437 (1968).
21. A. Lizana, J. Campos, A. van Eeckout, *et al.*, "Influence of temporal averaging in the performance of a rotating retarder imaging Stokes polarimeter," Opt. Express **28**(8), 355623 (2020).
22. A.V. Ryzhkov and D.S. Zrnic, *Radar polarimetry for weather observations*, Ed. (Springer, 2019).
23. D.V. Cotton, D.L. Buzasi, C. Aerts, *et al.*, "Polarimetric detection of non-radial oscillation modes in the β Cephei star β Crucis," Nat. Astron. **6**(1), 154–164 (2022).
24. M.A. Báez-Chorro and B. Vidal, "Single trace terahertz spectroscopic ellipsometry," Opt. Express **27**(24), 35468 (2019).
25. C. Zhang, S. Horder, T.K. Lee, *et al.*, "Development of polarization speckle based on random polarization phasor sum," J. Opt. Soc. Am. A **36**(2), 277 (2019).
26. M.F. Ramos, N. A. Silva, N. J. Muga, *et al.*, "Full polarization random drift compensation method for quantum communication," Opt. Express **30**(5), 6907 (2022).
27. B. Vidal, T. Mengual, C. Ibáñez-López, *et al.*, "Optical Beamforming Network based on Fiber Optical Delay Lines and Spatial Light Modulators for Large Antenna Arrays," IEEE Photonics Technol. Lett. **18**(24), 2590–2592 (2006).
28. Y. Yan, H. Ma, and Z. Jin, "Reducing polarization-fluctuation induced drift in resonant fiber optic gyro by using single-polarization fiber," Opt. Express **23**(3), 20022009 (2015).